Eur. Phys. J. C (2018) 78:266
https://doi.org/10.1140/epjc/s10052-018-5736-x

THE EUROPEAN PHYSICAL JOURNAL C

Regular Article - Experimental Physics

Cavity optomechanical spectroscopy constraints chameleon dark energy scenarios

Jian Liu[1,2], **Ka-Di Zhu**[1,2,a]

[1] Key Laboratory of Artificial Structures and Quantum Control (Ministry of Education), School of Physics and Astronomy, Shanghai Jiao Tong University, 800 DongChuan Road, Shanghai 200240, China
[2] Collaborative Innovation Center of Advanced Microstructures, Nanjing, China

Received: 30 September 2017 / Accepted: 12 March 2018 / Published online: 28 March 2018

Abstract The chameleon scalar field is a matter-coupled dark energy candidate with the screening mechanisms. In the present paper,we propose a quantum cavity optomechanical scheme to detect the possible signature of chameleons via the optical pump-probe spectroscopy. Compare to the previous experiment the sensitivity can be improved by the using of electrostatic shield and a pump-probe scheme to read the weak frequency splitting. We expect that this work will be a useful addition to the current literature on proposals to detect effects of dark energy.

1 Introduction

The nature of dark energy is a central mystery in cosmology, one possibility is that it consists of the scalar fields which may drive the acceleration of the expansion of the universe directly. This new light degrees of freedom will couple to matter fields and leads to long-range fifth forces [1]. But this new forces have not yet been detected on earth or in the solar system [2,3]. One way to alleviate this tension between theory and observation is through the introduction of screening mechanisms. The archetype of this screening mechanism is the chameleon model [4–6] which proposes that the coupling to matter depends on the local environmental matter density. In dense regions, such as in the laboratory, the coupling is very small, and the resulting force mediated by the chameleon is short ranged, shielding the chameleon interaction from detection. In regions of low density, such as in space, the coupling can be much stronger, and the resulting force mediated by the chameleon is long ranged. In a laboratory vacuum, the extremely low density ensures that sufficiently small objects are not screened from the scalar field and thus the force arising from the dark energy scalar could become significantly stronger. There have been a number of ways for probing the chameleon screening mechanism in the laboratory proposed or implemented in high vacuum, which have made efforts to derive new limits on the chameleon parameters. These include torsion-balance experiments [7,8], gravity resonance spectroscopy [9,10]. Recent searches using microscopic test masses such as atom, neutron [11–16] and the levitated microspheres [17] often provide the strongest constraints.

On the other hand, optomechanical coupling between the electromagnetic degrees of freedom and the mechanical motion of mesoscopic objects are promising approaches for studying the transition of a macroscopic degree of freedom from the classical to the quantum regime [18]. These systems can also be of considerable technological for improved measurements of displacements [19], forces [20] and masses [21]. Recently, the optical pump-probe technique has become a popular topic, which affords an effective way to investigate the light-matter interaction. Most recently, this optical pump-probe scheme has also been realized experimentally in cavity optomechanical systems [22–24]. Several phenomena have been demonstrated in different kinds of optomechanical systems based on the optical pump-probe technology such as optomechanically induced transparency [25], the large change in light velocity [26], optically-tunable delay [27], and light storage [28]. The mechanism underlying these effects can be explained as the four-wave mixing (FWM) process. The optical pump-probe technology uses a strong pump laser to stimulate the system to generate coherent optical effect while used the weak laser for probing. This method is of great interest for applications in nonlinear optical measurement within the cavity optomechanical system.

In this paper, we present a novel proposal to probe dark energy in an all-optical domain based on double levitated microparticles coupled to the cavity. We focus on chameleon scalar field theories, though our methods and results can be

[a] e-mail: zhukadi@sjtu.edu.cn

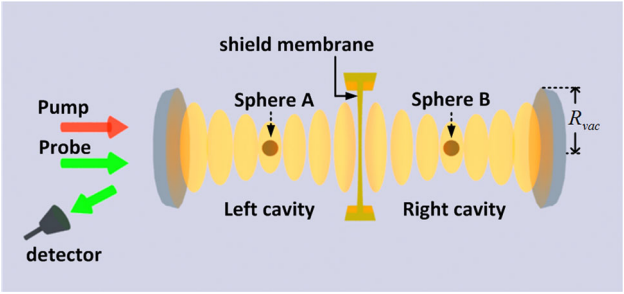

Fig. 1 Schematic diagram for probing the CIC. The vacuum cavity is driven by a strong pump pulse and a weak probe pulse. The optical levitated Silica microspheres with radii of 3 μm are separated by the distance of 80 μm form their mass centers. A shield membrane is placed between them to minimize the electromagnetic background forces

generalized to other theories with screening mechanisms. The remainder of the paper is organized as follows. Section 2 describes the theoretical model. Section 3 gives discussions about the measurement mechanism: (1) once the chameleons appear in the vacuum cavity, the probe spectrum will present an asymmetric splitting, which strongly reveals the chameleon induced coupling (CIC), namely, a signal indicative of the dark energy; (2) with optical optomechanical system, very tiny splitting in mechanical frequency could be readout optically. At last we derive new constraints on the chameleon parameters from existing experiments. Section 4 studies the background forces and limits in measurement. We suggest effective methods to eliminate the electrostatic force background and then check the frequency stability for thermomechanical noise. The last section contains the summary of the main results of the present work. The proposed scheme can be used to rule out large regions of the chameleon parameter space and to detect the fifth force due to the dark energy field in the laboratory.

2 Theory framework

We consider the two microspheres are placed inside a vacuum cavity consisting of two fixed mirrors. As shown in Fig. 1, the approach is based on optically trapping a microsphere with low natural mechanical frequency in the anti-node of an optical standing wave. The dielectric microsphere is attracted to the anti-node of the field. The resulting gradient in the optical field provides a sufficiently deep optical potential well which allows the particle to be confined in a number of possible trapping sites, with precise localization due to the optical standing wave [29–32]. We use the two spheres with the same radius R_i, density ρ_i, and mass $M_i (i = 1, 2)$. A shield membrane is placed between the sphere A and sphere B to minimize the electrostatic and Casimir background forces by preventing direct ac coupling between the masses. We use a silicon die which is etched into a frame bearing a 1 μm thick membrane of silicon nitride across an area of $\sim 1\,\mathrm{mm}^2$. The entire shield wafer die, including the membrane, is coated with gold on both sides, Because of the geometry and the tensile stress in the membrane [33], the membrane is expected to be sufficiently stiff. Previous experimental works have been successful at testing gravity at ultrashort distances by use of the Faraday shield [34,35], and similar techniques may work for the setup proposed here. Thus the experiment's force noise is presently induced by the electromagnetic interaction between the shield and the microspheres as we will discuss at last. The shield separates the left side of the cavity from the right side. In our model, the left cavity modes are strongly driven by the pump and probe pulses. Since the shielding membrane is apparently fully reflecting, we don't pump the right cavity which only provides the optical trapping of the sphere B.

In what follows we focus on an one-dimensional (1D) model. The Hamiltonian of the left cavity mode is $\hbar\omega_c\hat{a}^+\hat{a}$, here $\hat{a}$ is the annihilation operator for the cavity (frequency ω_c, damping rate κ). The trapped microspheres are treated as quantum-mechanical harmonic oscillators and their Hamiltonian can be regarded as $\hbar\omega_1\hat{o}_A^+\hat{o}_A$ and $\hbar\omega_2\hat{o}_B^+\hat{o}_B$, respectively. Here $\hat{o}_A$ and $\hat{o}_B$ are the annihilation operators of the two mechanical modes. We use ω_i and γ_i to denote their intrinsic frequencies and mechanical damping rates respectively. The simultaneous presence of a pump pulse and a probe pulse generates a radiation pressure force at the beat frequency, which drives the motion of the oscillator near its resonance frequency. The Hamiltonian of the interaction of the dielectric objects with the cavity fields is provided by optomechanical coupling $\hbar g\hat{a}^+\hat{a}(\hat{o}_A^+ + \hat{o}_A)$ [32], where g is the optomechanical coupling rate. Therefore the Hamiltonian of the system, in a frame rotating with the input laser frequency, is then given by

$$H = \hbar\Delta_{pu}\hat{a}^+\hat{a} + \hbar\omega_1\hat{o}_A^+\hat{o}_A + \hbar\omega_2\hat{o}_B^+\hat{o}_B + \hbar g\hat{a}^+\hat{a}(\hat{o}_A^+ + \hat{o}_A) - i\hbar\Omega_p(\hat{a} - \hat{a}^+) - i\hbar\Omega_{pr}(\hat{a}e^{i\delta t} - \hat{a}^+e^{-i\delta t}) + H_{int}, \quad (1)$$

where $\Delta_{pu} = \omega_c - \omega_p$ is pump-cavity detuning, $\delta = \omega_{pr} - \omega_p$ is the pump-probe detuning. We also introduce the Rabi frequency of the pump field and the probe field inside the cavity $\Omega_p = \sqrt{2P_p\kappa/\hbar\omega_p}$ and $\Omega_{pr} = \sqrt{2P_{pr}\kappa/\hbar\omega_{pr}}$, where P_p is the pump power, P_{pr} is the power of the probe field, respectively. H_{int} denotes the chameleon potential energy between the two levitated microspheres as we will discuss below.

A chameleon scalar field [4] is characterized by an effective potential density $V_{eff}(\phi) = V(\phi) + A(\phi)\rho_i$.The self-interaction $V(\phi) = \Lambda^{4+n}\phi^{-n}$ is characterized by strength of the self interaction Λ. The chameleons can drive the cosmic acceleration observed today if Λ is close to the cosmological-constant scale, $\Lambda \simeq 2.4$ meV. The coupling function to matter $A(\phi) = e^{\phi/M}$ is characterized by an energy scale

M, which is expected to be below the Planck mass. The chameleon profile due to an arbitrary static distribution of matter can be obtained by solving the non-linear Poisson equation $\nabla^2\phi = \partial V_{eff}/\partial\phi$.

For large global objects, the chameleon field with distance $r > R_i$ from the center is to a good approximation entirely determined by the contribution from infinitesimal volume elements lying within a thin shell of thickness ΔR_i. In that case, the object is said to be screened. For small objects, in the sense that $\Delta R_i/R_i > 1$, do not have a thin shell. Thus, their entire volume contributes to the field outside and the object is said to be unscreened. According Ref. [4], the exterior solution for a compact object is given by

$$\phi(r) = -\frac{M_i}{4\pi Mr}e^{-r/R_{vac}} + \phi_{vac} \quad \text{if } \frac{\Delta R_i}{R_i} > 1, \tag{2}$$

$$\phi(r) = -\frac{M_i}{4\pi Mr}\frac{3\Delta R_i}{R_i}e^{-r/R_{vac}} + \phi_{vac} \quad \text{if } \frac{\Delta R_i}{R_i} \ll 1. \tag{3}$$

The shell thickness can be defined as $\Delta R_i = M\phi_{vac}/\rho_i R_i$. ϕ_{vac} is the background value of ϕ inside the vacuum cavity, which has the form $\phi_{vac} = \zeta[n(n+1)\Lambda^{4+n}R_{vac}^2]^{1/(n+2)}$, where R_{vac} equals to the radius of the cavity mirrors. The proportionality constant ζ is determined by numerically solving the equation of motion in the vacuum chamber. In Ref. [16], it was found that ζ is largely sensitive to the assumed chamber geometry. Specifically, for $n = 1$ and the dark energy value $\Lambda = 2.4$ meV, one finds $\zeta = 0.68$ for a cylinder cavity. Dropping the irrelevant constant in the Eqs. (2) and (3), the resulting potential energy is

$$V(r) = -\lambda_i^2\frac{M_i^2}{4\pi M^2}\frac{e^{-r/R_{vac}}}{r}, \tag{4}$$

with

$$\lambda_i = \begin{cases} 1 & screened \\ 3M\phi_{vac}/\rho_i R_i^2 & unscreened. \end{cases}$$

The separation distance can be regarded as $r = r_0 + x_1 - x_2$, where $x_{1,2}$ denote the displacements of mechanical oscillators from their equilibrium positions, r_0 denotes the distance between the equilibrium positions. In our scheme the two levitated microspheres are separated by a distance of $r_0 = 80\ \mu$m, corresponding to the dark energy scale of $\Lambda = 2.4$ meV. Expanding Eq. (4) in the condition of $|x_1|, |x_2| \ll r_0$ and working to the lowest order, we can obtain the term of chameleon potential as

$$V(r) \approx \frac{-\lambda_i^2 M_i^2}{4\pi M^2}\left[\frac{1}{r_0} - \frac{x_1 - x_2}{r_0^2} + \frac{(x_1 - x_2)^2}{r_0^3} - \cdots\right] \cdot \left[1 - \frac{r}{R_{vac}} + \cdots\right]. \tag{5}$$

The first term is constant. The second term represents a steady force does not affect the interactional dynamics. The term proportional to x_1x_2 represents the lowest-order coupling between the microspheres' motions. At the distances of interest here, $r/R_{vac} \ll 1$. In the regime of $\omega_c, \omega_i \gg g$ the Hamiltonian of gravitational interaction can be obtained by quantizing mechanical oscillators within rotating wave approximation [36]

$$H_{int} = -\lambda_i^2\frac{M_i^2}{2\pi M^2 r_0^3}\vec{x_1}\vec{x_2} \approx \hbar\Psi(\hat{o}_A^+\hat{o}_B + \hat{o}_A\hat{o}_B^+), \tag{6}$$

and

$$\Psi = -\frac{\lambda_i^2}{2\pi}\frac{M_i^2}{M^2}\frac{1}{r_0^3\sqrt{M_i^2}\sqrt{\omega_i^2}} = -\frac{\lambda_i^2}{2\pi\omega_i r_0^3}\frac{M_i}{M^2}. \tag{7}$$

The coefficient Ψ can be defined as the chameleon induced coupling (CIC) strength which reveals the chameleonic interaction between the two coupled oscillators.

Substituting Eqs. (6) and (7) into Eq. (1), we define the operator $s_{A,B} = \hat{o}_{A,B}^+ + \hat{o}_{A,B}$ and deal with the mean response of the system to the probe field in the presence of the coupling. Let $\langle\hat{a}\rangle$, $\langle\hat{a}^+\rangle$ and $\langle s_{A,B}\rangle$ be the expectation values of operators $\hat{a}$, $\hat{a}^+$ and $s_{A,B}$, respectively. According to the Heisenberg equation of motion and the commutation relations $[\hat{a}, \hat{a}^+] = 1$, $[\hat{o}, \hat{o}^+] = 1$, the temporal evolutions of $\hat{a}$ and $s_{A,B}$ can be obtained and the corresponding equations are given by adding the damping terms

$$\frac{d\langle\hat{a}\rangle}{dt} = -(i\Delta_{pu} + \kappa)\langle\hat{a}\rangle + ig\langle S_A\rangle\langle\hat{a}\rangle + \Omega_p + \Omega_{pr}e^{-i\delta t}, \tag{8}$$

$$\frac{d^2\langle s_A\rangle}{dt^2} + \gamma_1\frac{d\langle s_A\rangle}{dt} + (\omega_1^2 + \Psi^2)\langle s_A\rangle - \Psi(\omega_1 + \omega_2)\langle s_B\rangle = 2g\omega_1\langle\hat{a}^+\rangle\langle\hat{a}\rangle, \tag{9}$$

$$\frac{d^2\langle s_B\rangle}{dt^2} + \gamma_2\frac{d\langle s_B\rangle}{dt} + (\omega_2^2 + \Psi^2)\langle s_B\rangle - \Psi(\omega_1 + \omega_2)\langle s_B\rangle = -2g\Psi\langle\hat{a}^+\rangle\langle\hat{a}\rangle. \tag{10}$$

To solve these equations, we make the ansatz as follows:

$$\langle\hat{a}(t)\rangle = a_0 + a_+e^{-i\delta t} + a_-e^{i\delta t}, \tag{11}$$

$$\langle s_A(t)\rangle = s_{A0} + s_{A+}e^{-i\delta t} + s_{A-}e^{i\delta t}, \tag{12}$$

$$\langle s_B(t)\rangle = s_{B0} + s_{B+}e^{-i\delta t} + s_{B-}e^{i\delta t}. \tag{13}$$

Substituting Eqs. (11)–(13) into Eqs. (8)–(10), respectively, equating terms with the same time dependence, and working to the lowest order in Ω_{pr} but to all orders in Ω_p, we can obtain

$$a_0 = \frac{\Omega_p}{i\Delta_{pu} + \kappa - i\delta - igs_{A0}}, \tag{14}$$

$$a_+ = \frac{\Omega_{pr} + ia_0gs_{A+}}{i\Delta_{pu} + \kappa - i\delta - igs_{A0}}, \tag{15}$$

$$a_- = \frac{ia_0gs_{A-}}{i\Delta_{pu} + \kappa + i\delta - igs_{A0}}, \tag{16}$$

and

$$(\omega_1^2+\Psi^2)s_{A0}-\Psi(\omega_1+\omega_2)s_{B0}=2g\omega_1 a_0^2, \tag{17}$$

$$s_{A+}=\frac{\Psi(\omega_1+\omega_2)s_{B+}+2g\omega_1(a_0^* a_+ + a_0 a_-^*)}{-\delta^2-i\gamma_1\delta+\omega_1^2+\Psi^2}, \tag{18}$$

$$s_{A-}=\frac{\Psi(\omega_1+\omega_2)s_{B-}+2g\omega_1(a_0^* a_- + a_0 a_+^*)}{-\delta^2+i\gamma_1\delta+\omega_1^2+\Psi^2}, \tag{19}$$

$$(\omega_2^2+\Psi^2)s_{B0}-\Psi(\omega_1+\omega_2)s_{A0}=-2g\Psi a_0^2, \tag{20}$$

$$s_{B+}=\frac{\Psi(\omega_1+\omega_2)s_{A+}-2g\Psi(a_0^* a_+ + a_0 a_-^*)}{-\delta^2-i\gamma_2\delta+\omega_2^2+\Psi^2}, \tag{21}$$

$$s_{B-}=\frac{\Psi(\omega_1+\omega_2)s_{A-}-2g\Psi(a_0^* a_- + a_0 a_+^*)}{-\delta^2+i\gamma_2\delta+\omega_2^2+\Psi^2}. \tag{22}$$

Solving Eqs. (14)–(22), we obtain in the steady state,

$$a_+=\Omega_{pr}\frac{Z(\Gamma-\chi)+U\omega_0}{Z(\Gamma^2-\chi^2)+2\chi U\omega_0}, \tag{23}$$

and the population ω_0 can be resolved by

$$\Omega_{pu}^2=[\kappa^2+(\Delta_{pu}-gS_{A0})^2]\omega_0, \tag{24}$$

with $\Gamma=\kappa-i\delta$, $\chi=i\Delta_{pu}-igs_{A0}$, $Y_j=-\delta^2-i\gamma_i\delta+\omega_i^2+\Psi^2(i=1,2)$, $Z=Y_1Y_2-\Psi^2(\omega_1+\omega_2)^2$, $U=2ig^2\omega_1 Y_2-2ig^2\Psi^2(\omega_1+\omega_2)$ and s_{A0}, s_{B0} can be resolved by

$$(\omega_1^2+\Psi^2)s_{A0}-\Psi(\omega_1+\omega_2)s_{B0}=2g\omega_1\omega_0, \tag{25}$$

$$(\omega_2^2+\Psi^2)s_{B0}-\Psi(\omega_1+\omega_2)s_{A0}=-2g\Psi\omega_0. \tag{26}$$

The transmission of the probe beam, defined as the ratio of the output and input field amplitudes at the probe frequency is then given by [18]

$$t(\omega_{pr})=\frac{\Omega_{pr}/\sqrt{2\kappa}-\sqrt{2\kappa}a_+}{\Omega_{pr}/\sqrt{2\kappa}}=1-2\kappa a_+/\Omega_{pr}. \tag{27}$$

3 Forecasts and constraints

To illustrate the experimental feasibility of the proposal, we will choose a set of experimental parameters.

(1) Dielectric object. We assume microspheres fabricated from fused silica with a radius $R_i=3\,\mu$m, density $\rho_i=2.3\,\mathrm{g/cm^3}$, and a dielectric constant $\epsilon=2$. (2) Cavity. We assume a low-finesse cylinder cavity of length $L=10$ cm, the radius of mirrors $R_{vac}=5$ cm, and finesse $F_c=10$ leading to a cavity decay rate $\kappa=c\pi/2F_cL=5\times10^8$ Hz. Then we obtain the standard optomechanical coupling rate $g\approx0.25$ Hz with waist of the trapping field $W=120\,\mu$m [37]. (3) Lasers. The cavity is impinged by a pump pulse of power $P_p=\Omega_p^2\hbar\omega_c/2\kappa=3\times10^{-5}$ W with wavelength $\lambda=1064$ nm, and we scan the probe frequency across the pump frequency in the spectrum. We assume the probe pulse of power $P_{pr}=10^{-7}$ W and the pulse frequency $\sim\omega_i\,(10^5$ Hz).

Taking a standing wave with wave number σ, to lowest order near an antinode the potential corresponds to a harmonic oscillator with mechanical frequency [32]

$$\omega_i=\left(\frac{6\sigma^2 I_0}{\rho_i c}\mathrm{Re}\frac{\epsilon-1}{\epsilon+2}\right)^{1/2}. \tag{28}$$

Here I_0 is the intracavity field intensity. Then we get $\omega_i=100$ kHz with $I_0=10^{-2}\,\mathrm{W/\mu m^2}$. In high vacuum, the dominant noise forces acting on the levitated sphere are collisions with the air molecules, thus the mechanical damping rate one would get for the optical trapping is solely depend on the properties of the background gas [38],

$$\gamma_i=\frac{3P}{R_i\rho_i v}. \tag{29}$$

Here $v=\sqrt{k_BT/m_{gas}}$ is the thermal velocity of the gas molecules, P the gas pressure.

The lower pressure limit of sputter-ion pumps is in the range of 10^{-11} mbar. Lower pressures in the range of 10^{-12} mbar can only be achieved when the sputter-ion pump works in a combination with other pumping methods. Well established are the combinations of a sputter-ion pump with a titanium sublimation pump (TSP) or a non-evaporable getter module (NEG). An ultimate pressure of about 2×10^{-12} Torr was achieved inside 12 m long chambers made of Al alloy and pumped by a linear non-evaporable getter (NEG) strip and a sputter-ion pump of about $50\,\mathrm{l\,s^{-1}}$ nominal speed [39]. This pressure could be further reduced to about 5×10^{-13} Torr by increasing the pumping speed for Ar and CH4, not pumped by getters, with the addition of five more sputter-ion pumps of the same size [40]. Pressures in the low 10^{-14} Torr range have been reproducibly achieved in a 3m long vacuum chamber [41]. In our considerations, a conservative value is taken $P=10^{-10}$ Torr, which is usually required for achieving ultrahigh-Q mechanical oscillators and the ultrasensitive measurements in the levitated optomechanical system [19,20,32,42,43]. Then we find $\gamma_i=10^{-7.8}$ Hz in the room-temperature gas, indicating that ideal oscillators can be essentially decoupled from their thermal environment.

Compared with the previous scheme to detect chameleons via the force-distance properties by the levitated microspheres as discussed in Ref. [17], the distinct difference of our scheme is focused on the quantum optomechanics detection using optical nonlinear spectrum. The chameleon induced coupling strength Ψ can be obtained from Eq. (7) by setting different energy scales M and Λ. For both the test and source objects are unscreened. The CIC strength can be expressed as

$$\Psi_u(M)=-\frac{M_i}{2\pi\omega_i r_0^3 M^2}. \tag{30}$$

In Fig. 2, we have plotted the transmission $|t|^2$ of the probe beam versus detuning at resonance $\delta-\omega_i$ for different

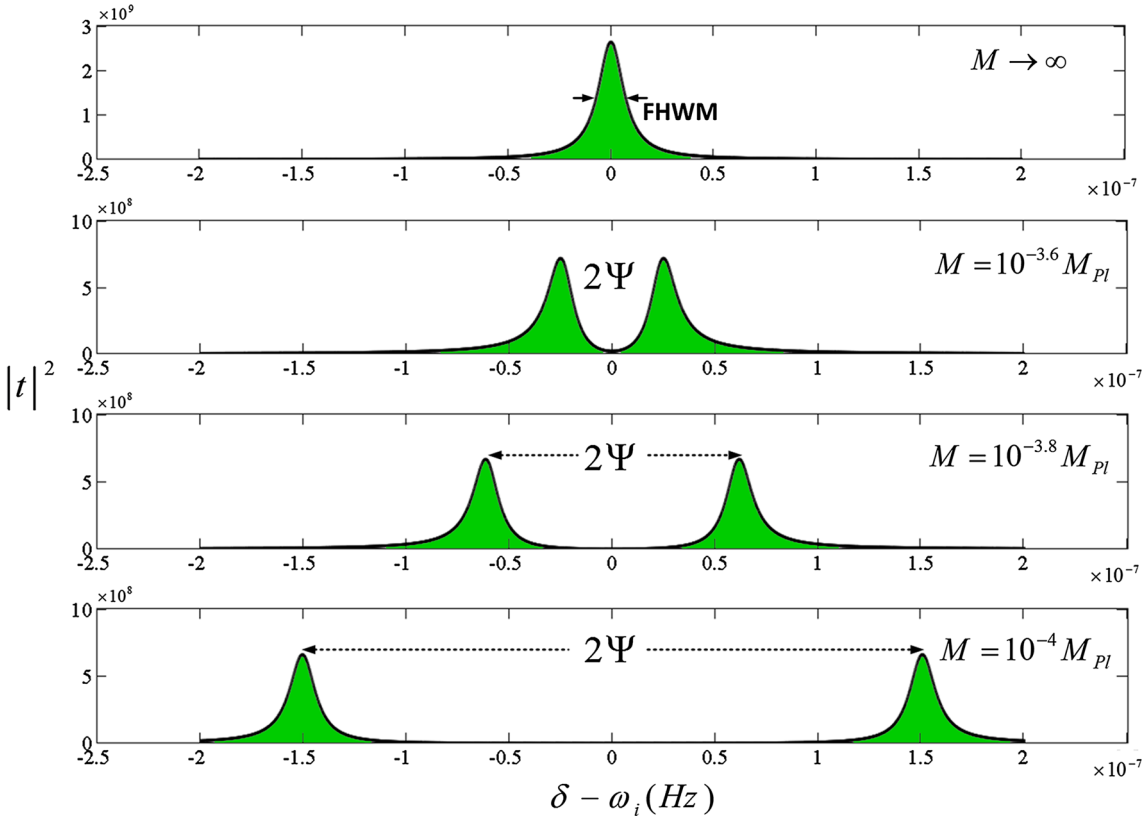

Fig. 2 The plot of the probe transmission spectrum as a function of detuning $\delta - \omega_i$ with different chameleon -matter coupling strength M in the conditions of $r_i = 3\ \mu$m, $r_0 = 80\ \mu$m. The peak splitting caused by chameleon coupling between objects Ψ can be well recognized in the spectrum.The other parameters are $\omega_i = 100$ kHz, $g = 0.25$ Hz, $\kappa = 5 \times 10^8$ Hz, $\Omega_p = 1$ THz

M. Without the presence of chameleons ($M \to \infty$), we find a enhanced peak located at the fundamental frequency ω_i of the two oscillators as shown in the first picture. As the chameleons appear with the strength $M = 10^{-3.6} M_{Pl}$, the probe transmission spectrum will present an asymmetric splitting depicted by the second picture. Here $M_{Pl} = 1/\sqrt{8\pi G}$ is the reduced Planck mass. The two peaks displaying in Fig. 2 for given energy scales $M = 10^{-3.8} M_{Pl}$ and $M = 10^{-4} M_{Pl}$ represent the chameleon interactions between the two spheres. The splitting becomes larger with increasing M. Thus the dark energy signature can be observed distinctly in the pump-probe spectrum. The splitting distance D has a simple relationship with the CIC strength Ψ via $\Psi = D/2$, which provides a straight way to measure the CIC strength on the spectrum. According to the Eq. (30), the minimal detectable field-matter coupling strength $M_{\min}$ is mainly determined by the full width at half maximum (FWHM) of the resonance peak on the probe spectrum. Considering $D_{\min} = FWHM \approx 10^{-7.8}$ Hz in Fig. 2, one can obtain $\Psi_{\min} \approx 8 \times 10^{-9}$ Hz, hence $M_{\min} = 10^{-3.5} M_{Pl}$.

The simultaneous presence of a pump field and a probe field generates a radiation pressure force at the beat frequency, which drives the motion of the oscillator near its resonance frequency. In the Fig. 3, $|N\rangle$, $|n_1\rangle$ and $|n_2\rangle$ denote the number states of the cavity photon, and sphere A and sphere B phonons, respectively. $|N, n_1, n_2\rangle \leftrightarrow |N+1, n_1, n_2\rangle$ transition changes the cavity field, $|N+1, n_1, n_2\rangle \leftrightarrow |N, n_1+1, n_2\rangle$ transition is caused by the radiation pressure coupling. In a double oscillators system,the coupling between two microspheres adds a fourth level. The energy-level can be modified by the chameleonic interaction. The CIC breaks down the symmetry of the optomechanical induced interference, and thereby the single pump-probe transparency window is split into two transparency windows, which yields the chameleon induced optical nonlinearity.

For the both objects become screened, here the CIC strength can be obtained by

$$\Psi_s(\Lambda) = -\frac{6\phi_{vac}^2}{\omega_i r_0^3 \rho_i R_i}. \tag{31}$$

Thus in this case, the CIC strength is completely independent of the field-matter interactional strength M, but be changed by the strength of the self interaction Λ. Substituting the minimal detectable CIC strength $\Psi_{\min} = D_{\min}/2 \approx 8 \times 10^{-9}$ Hz into Eq. (31), we find that the dark energy scale

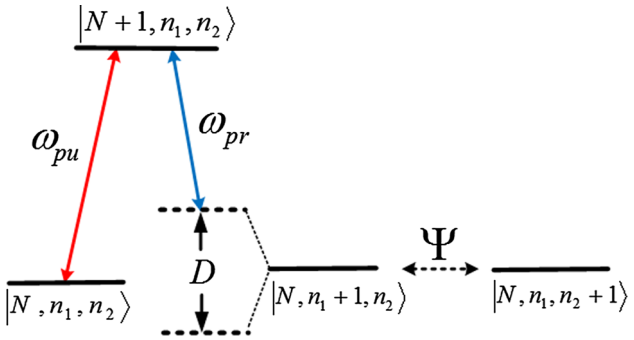

Fig. 3 Schematic of the energy-level diagram the energy-level splitting. $|N, n_1 + 1, n_2\rangle \leftrightarrow |N, n_1, n_2 + 1\rangle$ transition is induced by the chameleon coupling

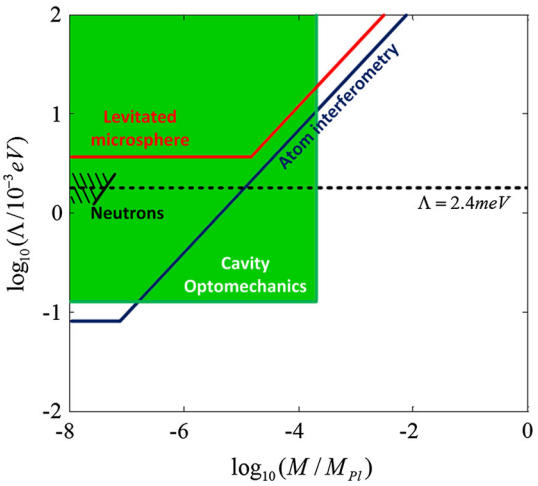

Fig. 4 The expected constraint in the $M/M_{Pl} \sim \Lambda$ plane for $n = 1$, the regions in the rectangle (indicated by green) will be excluded. The horizontal line marks the range around $\Lambda = 2.4$ meV, where the chameleon field would reproduce the current cosmic acceleration. Recent constraints from atom interferometry are shown by the blue lines [13,14]. The black line indicates limits from neutron interferometry (indicated by shadows) [11]. The constraint of the levitated microsphere experiment [17] are denoted by the red line. Our results are about one or two orders of magnitude stronger than the ones from atom interferometry at the dark energy range

can be measured down to a precision of the order of $\Lambda \sim 10^{-1}$ meV.

The Eqs. (30), (31) predict the CIC between the levitated microspheres due to the screening mechanisms in a vacuum chamber. Figure 4 shows our bounds for theories with the exponent $n = 1$ compared to existing experimental limits on chameleon interactions. The $\Lambda - M$ area of the green will be excluded by the quantum optomechanical detection. The system excludes the range $M \leqslant 10^{-3.6} M_{Pl}$ for the all range of Λ. This constraint is about one to two orders of magnitude stronger than the ones from atom interferometry at the range of $\Lambda = 2.4$ meV [13].

4 Background noise

4.1 Background forces

One can place a stiff metallized shield between the drive and test masses to minimize the effects of electromagnetic forces by preventing direct ac coupling between the masses. This method lead to the conclusion that the experiment's force resolution is presently limited by an environmental effect, most likely an electrostatic interaction between the shield and the test mass. Basically, there is a relatively large background force present at all times between the microspheres and shield membrane. Although electrically neutral microspheres are used, they still contain 10^{14} charges and interact primarily as electric dipoles.

To study the background forces noise in the system, we focus on the left cavity where the "sphere A" strongly interacts with the shield membrane. We map the system onto the cavity optomechanics in which the microsphere and the shield are dipole–dipole coupled. The interactional energy between them can be written as

$$U = -\frac{\mu_i \mu_s}{2\pi\varepsilon_0 R_0^3}. \tag{32}$$

Here μ_i and μ_s are the dipole moments of the levitated microsphere and the shield membrane. The separation distance can be regarded as $R_0 = d_0 + x_1 - x_s$, where x_s denote the displacements of shield from their equilibrium positions, d_0 denotes the distance between the equilibrium positions. The Hamiltonian of electrostatic interaction can be obtained by quantizing mechanical oscillators within rotating wave approximation

$$H_E = -\frac{\mu_i \mu_s}{\pi\varepsilon_0 d_0^5} \vec{x_1}\vec{x_s} \approx -\hbar\Theta(\hat{o}_A^+ \hat{o}_S + \hat{o}_A \hat{o}_S^+), \tag{33}$$

and

$$\Theta = -\frac{\mu_i \mu_s}{\pi\varepsilon_0 d_0^5} \frac{1}{\sqrt{M_i M_s}\sqrt{\omega_i \omega_s}}, \tag{34}$$

where $\hat{o}_S^+(\hat{o}_S)$ are the bosonic creation(annihilation) operators for the shield membrane with the oscillation frequency of ω_s and the mass M_s. The dipole moments of levitated microspheres are measured experimentally. According to the Ref. [17], we assume $\mu_i \approx 10^2$ e $\cdot$ μm and $\mu_s \approx 10^7$ e $\cdot$ μm. The measurement of the membrane's lowest mechanical resonance provides the lowest flexural resonance frequency $\omega_s \approx 130$ kHz [44]. If we trap the microsphere near the shield membrane with the distance $d_0 = 40$ μm, we can obtain the coupling $\Theta \approx 3 \times 10^{-3}$ Hz, which is about 5 order of magnitudes higher than the chameleon induced coupling rate Ψ.

The Hamiltonian of the system of is then given by

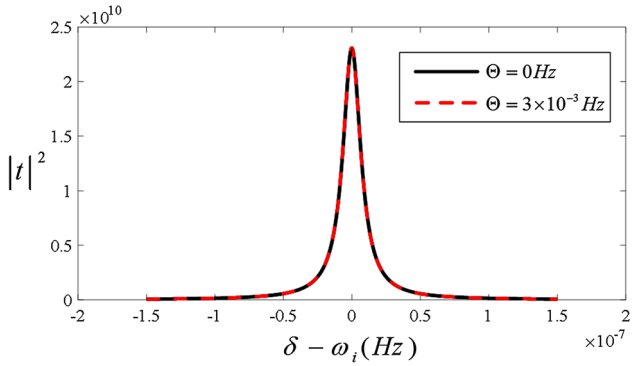

Fig. 5 The black curve shows the initial resonance of the levitated microsphere A, the red dash curve after considering the dipole force coupling between sphere A and the shield membrane which are separated by a distance of $d_0 = 40\ \mu$m. We assume the shield membrane's lowest mechanical resonance provides the lowest flexural resonance frequency $\omega_s = 130$ kHz. The result shows that the splitting is independent of the interactions between them. The other parameters are the same with that in Fig. 2

$$H = \hbar\Delta_{pu}\hat{a}^{+}\hat{a}+\hbar\omega_i\hat{o}_A^{+}\hat{o}_A + \hbar\omega_s\hat{o}_S^{+}\hat{o}_S + \hbar g\hat{a}^{+}\hat{a}(\hat{o}_A^{+} + \hat{o}_A) - i\hbar\Omega_p(\hat{a} - \hat{a}^{+}) - i\hbar\Omega_{pr}(\hat{a}e^{i\delta t} - \hat{a}^{+}e^{-i\delta t}) + H_E. \tag{35}$$

The Hamiltonian have the same expression with Eq. (1), thus we can manipulate it with the same means. In order to study the interaction between the microsphere and the shield, we depict the transmission of the probe beam as a function of the probe-pump detuning without or with the dipole–dipole force in Fig. 5. Without the presence of electrostatic force ($\Theta = 0$), we get an enhanced peak which is located at the fundamental frequency $\delta = \omega_i$. By applying the dipole–dipole interaction strength Θ, we then depict the probe spectrum by the red dashed line in Fig. 5. Although the interactional strength is very large($\Theta \sim 10^{-3}$ Hz), interestingly, the probe spectrum will not be charged, because of the separation of the drive frequency ω_s from the trapping frequency ω_i. That is to say, the dipole–dipole coupling can't induce an optomechanical splitting on the spectrum in the condition of $\omega_s \neq \omega_i$. Thus it is reasonable to ignore the electrostatic background noise in the system and the contribution of chameleons will be able to show itself clearly on the probe spectrum via the splitting as discussed before. We call this phenomenon as an optomechanical screening and we find any interaction between the shield and the test mass would likely be too small to make the shield deflect enough to drive the levitated microsphere a measurable splitting on spectrum.

Such a shield can screen the chameleon fifth force as well. The change in source mass position will result in a change $\Delta\phi$ in the field on the surface of the test mass. The suppression factor can defined as $f_s = \Delta\phi(shield)/\Delta\phi(non\text{-}shield)$. According to Ref. [8], f_s is approximately equal to $f_s \approx sech(2m_{eff}d_s)$, where d_s is the foil thickness, m_{eff} is the effective mass of the $\phi(\rho)$ fluctuations, it is given by

$$m_{eff}^2(\rho) \approx n(n+1)\Lambda^{-\frac{4+n}{1+n}}\left(\frac{\rho_i}{nM}\right)^{\frac{n+2}{n+1}}. \tag{36}$$

Here it is manifest that the effective mass is a function of the ambient density, ρ_i, and that it increases with increasing density, exactly as desired. The suppression factor is approximately equal to 1 in the case of $2m_{eff}d_s < 0.1$. In our scheme, we use a shield membrane of $d_s = 1\ \mu$m. Considering the dimensionless numbers $n = 1$ and the dark energy scale $\Lambda = 2.4$ meV, we can obtain $m_{eff}d_s \approx 4 \times 10^{-5}$ with the coupling strength $M_{pl}/M = 10^{-3}$. Thus $m_{eff}d_s \ll 0.1$ and the force suppression due to shielding membrane can be safely neglected.

Furthermore, the chameleon force depends on the size and geometry of the vacuum chamber as discussed in details in Ref. [16]. Hence we suggest that by comparing the interactions of two objects in different chamber geometry, we may be able to subtract out the common electromagnetic force background. According to Eq. (31) for $n = 1$, we have

$$\frac{\partial D}{\partial R_{vac}} = \frac{34\zeta^2}{\omega_i r_0^3 \rho_i R_i}\Lambda^{10/3}R_{vac}^{1/3}. \tag{37}$$

The sensitivity for the radius of the vacuum cavity can be defined as $\Delta R_{vac} = (\partial D/\partial R_{vac})^{-1}\Delta D$. Consider $\Delta D = 10^{-7.8}$ Hz, when $R_{vac} = 5cm$, $\Lambda = 2.4$ meV, we get $\Delta R_{vac} = 1.2\ \mu$m. Hence we can separate out the signals of the chameleons form strong electrostatic force background through changing the vacuum cavity radius by microns.

4.2 Thermal noise

The evaluation of the minimum measurable frequency shift, $\delta\omega$, limited by thermomechanical fluctuations of a nanoelectromechanical systems (NEMS) resonator can be expressed as [38]

$$\delta\omega = \sqrt{\frac{k_B T}{E_c}\frac{\omega_i \Delta f}{Q}}. \tag{38}$$

Here, k_B is Boltzmann's constant, T is the resonator temperature, Δf is the measurement bandwidth, Q is the quality factor of the microsphere which can be given by $Q = \omega_i/2\pi\gamma_i \approx 10^{12}$. $E_c = m\omega_i^2\langle x_c^2\rangle$ represents the maximum drive energy of the microsphere, where we defined $\langle x_c\rangle$ as the maximum rms level still consistent with producing a predominantly linear response. For a Gaussian field distribution, the nonlinear coefficients are given by $\xi = -2/W^2$ [45], Considering the beam waist radius $W = 120\ \mu$m, for small displacements $|x_c| \ll |\xi|^{-1/2} = 8 \times 10^{-5}$ m, the nonlinearity is negligible. In our considerations, x_c is taken to be 3 orders of magnitude smaller, we choose $x_c = 8 \times 10^{-8}$ m, thus the frequency stability will reach $\delta\omega = 1.5 \times 10^{-8}$ Hz with the measurement bandwidth $\Delta f = 10^{-5}$ Hz at the room

temperature ($T = 300\,\mathrm{K}$). Here, $\Delta f \approx 1/2\pi t_m$ and is dependent upon the measurement averaging time t_m, thus we get $t_m \approx 1.6 \times 10^4$ s.

5 Conclusion

We discuss dynamics of the chameleonic coupled quantum cavity optomechanical oscillators, then suggest feasible methods to detect the chameleon dark energy with high sensitivity based the pump-probe technology.Using two levitated microspheres in an ultrahigh-vacuum chamber, we reduced the screening mechanism. We find that the normal mode splitting can be observed due to the chameleonic induced coupling strength. The splitting distance has a simple linear relationship with the CIC strength, which strongly reveals the new light degrees of freedom coupled to matter fields. We use a stiff metallized shield to provide the attenuation of electrostatic and Casimir forces between two spheres, then discuss the background forces between the shield membrane and the levitated sensor. The splitting distance is independent of the interactions between them, leading an effective way to avoid strong background force noise. Moreover, several other methods are also proposed to minimize the noises.

Acknowledgements This work was supported by the National Natural Science Foundation of China (Nos. 11274230 and 11574206), the Basic Research Program of the Committee of Science and Technology of Shanghai (No. 14JC1491700).

References

1. A. Joyce, B. Jain, J. Khoury, M. Trodden, Beyond the cosmological standard model. Phys. Rep. **568**, 1 (2015)
2. J. Khoury, A. Weltman, Chameleon fields: awaiting surprises for tests of gravity in space. Phys. Rev. Lett. **93**, 171104 (2004)
3. D.F. Mota, D.J. Shaw, Evading equivalence principle violations, cosmological and other experimental constraints in scalar field theories with a strong coupling to matter. Phys. Rev. D **75**, 063501 (2007)
4. J. Khoury, A. Weltman, Chameleon cosmology. Phys. Rev. D **69**, 044026 (2004)
5. S.S. Gubser, J. Khoury, Scalar self-interactions loosen constraints from fifth force searches. Phys. Rev. D **70**, 104001 (2004)
6. D.F. Mota, D.J. Shaw, Strongly coupled chameleon fields: new horizons in scalar field theory. Phys. Rev. Lett. **97**, 151102 (2006)
7. D.J. Kapner, T.S. Cook, E.G. Adelberger, J.H. Gundlach, B.R. Heckel, C.D. Hoyle, H.E. Swanson, Tests of the gravitational inverse-square law below the dark-energy length scale. Phys. Rev. Lett. **98**, 021101 (2007)
8. A. Upadhye, Dark energy fifth forces in torsion pendulum experiments. Phys. Rev. D **86**, 102003 (2012)
9. T. Jenke, G. Cronenberg, J. Burgdörfer, L.A. Chizhova, P. Geltenbort, A.N. Ivanov, T. Lauer, T. Lins, S. Rotter, H. Saul, U. Schmidt, H. Abele, Gravity resonance spectroscopy constrains dark energy and dark matter scenarios. Phys. Rev. Lett. **112**, 151105 (2014)
10. A.N. Ivanov, R. Hollwieser, T. Jenke, M. Wellenzohen, H. Abele, Influence of the chameleon field potential on transition frequencies of gravitationally bound quantum states of ultracold neutrons. Phys. Rev. D **87**, 105013 (2013)
11. H. Lemmel, A.N. Ph Brax, T. Ivanov, G. Jenke, M. Pignol, T. Pitschmann, M. Potocar, M. Wellenzohn, H.Abele Zawisky, Neutron interferometry constrains dark energy chameleon fields. Phys. Lett. B **743**, 310 (2015)
12. K. Li, M. Arif, D.G. Cory, R. Haun, B. Heacock, M.G. Huber, J. Nsofini, D.A. Pushin, P. Saggu, D. Sarenac, C.B. Shahi, V. Skavysh, W.M. Snow, A.R. Young, Neutron limit on the strongly-coupled chameleon field. Phys. Rev. D **93**, 062001 (2016)
13. P. Hamilton, M. Jaffe, P. Haslinger, Q. Simmons, H. Müller, J. Khoury, Atom-interferometry constraints on dark energy. Science **349**, 849 (2015)
14. C. Burrage, E.J. Copeland, E.A. Hinds, Probing dark energy with atom interferometry. J. Cosmol. Astropart. Phys. **3**, 042 (2015)
15. S. Schlogel, S. Clesse, A. Fuzfa, Probing modified gravity with atom-interferometry: a numerical approach. Phys. Rev. D **93**, 104036 (2016)
16. B. Elder, J. Khoury, P. Haslinger, M. Jaffe, H. Müller, P. Hamilton, Chameleon dark energy and atom interferometry. Phys. Rev. D **94**, 044051 (2016)
17. A.D. Rider, D.C. Moore, C.P. Blakemore, M. Louis, M. Lu, G. Gratta, Search for screened interactions associated with dark energy below the 100 μm length scale. Phys. Rev. Lett. **117**, 101101 (2016)
18. M. Aspelmeyer, T.J. Kippenberg, F. Marquardt, Cavity optomechanics. Rev. Mod. Phys. **86**, 1391 (2014)
19. K.G. Libbrecht, E.D. Black, Toward quantum-limited position measurements using optically levitated microspheres. Phys. Lett. A **321**, 99 (2004)
20. A.A. Geraci, S.B. Papp, J. Kitching, Short-range force detection using optically cooled levitated microspheres. Phys. Rev. Lett. **105**, 101101 (2010)
21. W. Bin, K.D. Zhu, Nucleonic-resolution optical mass sensor based on a graphene nanoribbon quantum dot. Appl. Opt. **52**, 5816 (2013)
22. S. Weis, R. Rivière, S. Deléglise, E. Gavartin, O. Arcizet, A. Schliesser, T.J. Kippenberg, Optomechanically induced transparency. Science **330**, 1520 (2010)
23. J.D. Teufel, D. Li, M.S. Allman, K. Cicak, A.J. Sirois, J.D. Whittaker, R.W. Simmonds, Circuit cavity electromechanics in the strong-coupling regime. Nature **471**, 204 (2011)
24. A.H. Safavi-Naeini, T.P. Mayer Alegre, J. Chan, M. Eichenfield, M. Winger, Q. Lin, J.T. Hill, D.E. Chang, O. Painter, Electromagnetically induced transparency and slow light with optomechanics. Nature **472**, 69 (2011)
25. W. He, J.J. Li, K.D. Zhu, Coupling-rate determination based on radiation-pressure-induced normal mode splitting in cavity optomechanical systems. Opt. Lett. **35**, 339 (2010)
26. B. Chen, C. Jiang, K.D. Zhu, Slow light in a cavity optomechanical system with a Bose–Einstein condensate. Phys. Rev. A **83**, 055803 (2011)
27. J.J. Li, K.D. Zhu, A tunable optical Kerr switch based on a nanomechanical resonator coupled to a quantum dot. Nanotechnology **21**, 205501 (2010)
28. J.J. Li, K.D. Zhu, Spin-based optomechanics with carbon nanotubes. Sci. Rep. **2**, 903 (2012)

29. G. Ranjit, M. Cunningham, K. Casey, A.A. Geraci, Zeptonewton force sensing with nanospheres in an optical lattice. Phys. Rev. A **93**, 053801 (2016)
30. O. Romero-Isart, M.L. Juan, R. Quidant, J.I. Cirac, Entangling the motion of two optically trapped objects via timemodulated driving fields. New J. Phys. **12**, 033015 (2010)
31. N. Kiesel, F. Blaser, U. Delic, D. Grass, R. Kaltenbaek, M. Aspelmeyer, Cavity cooling of an optically levitated submicron particle. Proc. Natl. Acad. Sci. USA **110**, 14180 (2013)
32. D.E. Chang, C.A. Regal, S.B. Papp, D.J. Wilson, J. Ye, O. Painter, H.J. Kimble, P. Zoller, Cavity opto-mechanics using an optically levitated nanosphere. Proc. Natl. Acad. Sci. USA **107**, 1005 (2010)
33. A. Kaushik, H. Kahn, A.H. Heuer, Wafer-level mechanical characterization of silicon nitride MEMS. J. Microelectromech. Syst. **14**, 359 (2005)
34. J. Chiaverini, S.J. Smullin, A.A. Geraci, D.M. Weld, A. Kapitulnik, New experimental constraints on non-newtonian forces below 100 μm. Phys. Rev. Lett. **90**, 151101 (2003)
35. A.A. Geraci, S.J. Smullin, D.M. Weld, J. Chiaverini, A. Kapitulnik, Improved constraints on non-Newtonian forces at 10 microns. Phys. Rev. D **78**, 022002 (2008)
36. K.R. Brown, C. Ospelkaus, Y. Colombe, A.C. Wilson, D. Leibfried, D.J. Wineland, Coupled quantized mechanical oscillators. Nature **471**, 196 (2011)
37. O. Romero-Isart, A.C. Pflanzer, M.L. Juan, R. Quidant, N. Kiesel, M. Aspelmeyer, J.I. Cirac, Optically levitating dielectrics in the quantum regime: theory and protocols. Phys. Rev. A **83**, 013803 (2011)
38. K.L. Ekinci, Y.T. Yang, M.L. Roukes, Ultimate limits to inertial mass sensing based upon nanoelectromechanical systems. J. Appl. Phys. **95**, 2682 (2004)
39. C. Benvenuti, A new pumping approach for the large electron positron collider (LEP). Nucl. Instrum. Methods **205**, 391 (1983)
40. C. Benvenuti, J.P. Bojon, P. Chiggiato, G. Losch, Ultimate pressures of the large electron positron collider (LEP) vacuum system. Vacuum **44**, 507 (1993)
41. C. Benvenuti, P. Chiggiato, Obtention of pressures in the 10^{-14} torr range by means of a Zr–V–Fe non evaporable getter. Vacuum **44**, 511 (1993)
42. A. Arvanitaki, A.A. Geraci, Detecting high-frequency gravitational waves with optically levitated sensors. Phys. Rev. Lett. **110**, 071105 (2013)
43. D.E. Chang, K. Ni, O. Painter, H.J. Kimble, Ultrahigh-Q mechanical oscillators through optical trapping. New J. Phys. **14**, 045002 (2012)
44. J.D. Thompson, B.M. Zwickl, A.M. Jayich, F. Marquardt, S.M. Girvin, J.G.E. Harris, Strong dispersive coupling of a high-finesse cavity to a micromechanical membrane. Nature **452**, 72 (2008)
45. J. Gieseler, L. Novotny, R. Quidant, Thermal nonlinearities in a nanomechanical oscillator. Nat. Phys. **9**, 806 (2013)